Analysis of the atomic geometries of the $(10\bar{1}0)$ and $(11\bar{2}0)$ surfaces of CdSe by low-energy-electron diffraction and low-energy-positron diffraction

T.N. Horsky,* G.R. Brandes,† and K.F. Canter
Department of Physics, Brandeis University, Waltham, Massachusetts 02251

C.B. Duke and A. Paton
Xerox Webster Research Center, 800 Phillips Road, 0114-38D, Webster, New York 14580

D.L. Lessor
Pacific Northwest Laboratory, Richland, Washington 99352

A. Kahn, S.F. Horng, K. Stevens, and K. Stiles
Department of Electrical Engineering, Princeton University, Princeton, New Jersey 08544

A.P. Mills, Jr.
AT&T Bell Laboratories, Murray Hill, New Jersey 07974
(Received 9 January 1992)

The relaxed atomic geometries of the low-index cleavage surfaces of wurtzite-structure CdSe are determined via comparison of dynamical scattering calculations with measured low-energy-electron-diffraction (LEED) and low-energy-positron-diffraction (LEPD) intensities. Both surfaces are found to be relaxed in accordance with recently proposed geometries deduced from total-energy-minimization calculations. Since this analysis represents the use of LEPD for quantitative surface-structure determination, we discuss the experimental technique, the differences observed between LEPD and LEED, and the complementary nature of the two spectroscopies.

I. INTRODUCTION

In this paper we report the quantitative structure determination of both cleavage faces, $(10\bar{1}0)$ and $(11\bar{2}0)$, of a wurtzite-structure compound semiconductor. The analysis is of interest for three reasons. First, it extends to wurtzite-structure compound semiconductors the detailed analysis of surface atomic geometries that previously characterized zinc-blende structure materials.[1–3] Second, it confirms for the cleavage faces of wurtzite-structure compound semiconductors the surface-state-lowering mechanism of surface relaxation which had been established for the zinc-blende (110) surfaces.[4] Third, it establishes low-energy positron diffraction (LEPD) as not only being comparable to low-energy-electron diffraction (LEED) for the quantitative determination of surface atomic geometries, but also offering the possibility that it can provide more precise structural information than can be obtained with LEED alone.[5–7] Thus, it is useful to consider the context of the analysis from each of these perspectives.

While most III-V semiconductors exhibit zinc-blende structures, most II-VI compounds crystallize in the wurtzite form. Wurtzite-structure compound semiconductors exhibit two cleavage faces, the $(10\bar{1}0)$ and $(11\bar{2}0)$ surfaces, both of which are electrically neutral in that the surface atomic plane contains equal numbers of anions (Se) and cations (Cd). Early LEED intensity data on these surfaces of ZnO and CdS were reported by Mark *et al.*[8] Complete LEED intensity analysis structure determinations have been reported for the $(10\bar{1}0)$ surfaces of ZnO (Refs. 9 and 10) and CdSe.[11] Originally thought to exhibit truncated-bulk structures,[8] both the $(10\bar{1}0)$ and $(11\bar{2}0)$ surfaces are now known to exhibit large nearly bond-length-conserving relaxations with the anion displaced outward and the cation inward.[5–7,9–12] Schematic representations that illustrate the independent structural variables associated with these relaxations are given in Figs. 1 and 2 for the $(10\bar{1}0)$ and $(11\bar{2}0)$ surfaces, respectively.

The key feature of both surfaces is that, like the zinc-blende (110) surface, they can exhibit *bond-length-conserving relaxations* in which the local atomic coordination is altered significantly, e.g., from sp^3 to approximately p^3 for the anion (Se) and sp^2 for the cation (Cd). Therefore these surfaces can experience activationless relaxations in which the surface species move large distances (~ 1 Å) in order to achieve an energetically more favorable local hybridization.[2,4] This fact is thought to be responsible for the large relaxations on these surfaces. In contrast, large relaxations on the cleavage ("fracture") surfaces of cubic or rutile compounds because bond-length-conserving relaxations are not allowed due to the topography of these surfaces.[4,13] The present study was undertaken to validate or disprove this idea. The hypothesis that approximately bond-

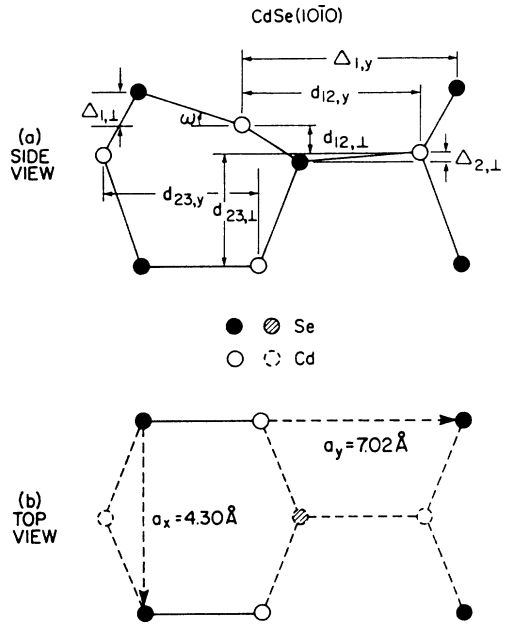

FIG. 1. Schematic indication of the independent structural variables for the (10$\bar{1}$0) surface of CdSe. $\Delta_{2,\perp} < 0$ corresponds to Cd higher than Se.

length-conserving relaxations lead to large relaxations characterized by sp^2-coordinated cations and distorted p^3-coordinated anions was advanced empirically for zinc-blende (110) surfaces[2] and extended to wurtzite structure ZnO,[14] ZnSe,[15] ZnS,[16] CdS,[17] and CdSe (Ref. 17) by tight-binding total-energy calculations. The latter predicted that if bond-length-conserving relaxations were permitted geometrically, they would occur by virtue of a surface-state lowering mechanism. Small bond-length contractions also occur, but most of the energy is gained by the rehybridization of the bonding of surface species accompanied by bond-angle distortions alone. Therefore the close correspondence between our experimentally determined geometries and the predicted[17] ones lends credence to the concept of universality of both the mechanism for the relaxations and the linear scaling of the final independent surface-structure parameters with the bulk lattice constants.[4]

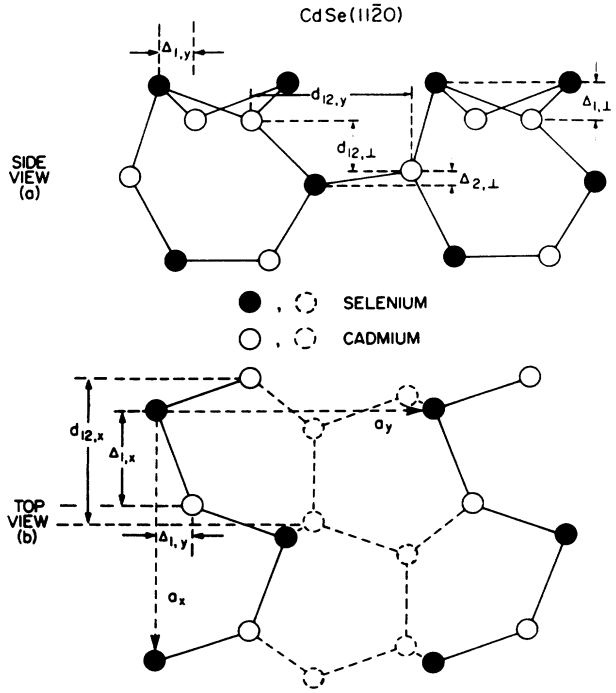

FIG. 2. Schematic indication of the independent structural variables for the (11$\bar{2}$0) surface of CdSe. $\Delta_{2,\perp} < 0$ corresponds to Cd higher than Se.

An observation of the positron equivalent of LEED, i.e., LEPD, was made by Rosenberg, Weiss, and Canter.[18] Their ability to produce finely focused positron beams was severely limited so that the resolution of the early LEPD results was below that of Davisson and Germer's LEED results obtained fifty years earlier.[19] The principal limitation of positron beams at that time was the inability to focus the low-energy (40–400 eV) positrons to the 1 mm diameter and 1° angular divergence typical of modern LEED studies, without at the same time aperturing the beam down to an unacceptably low flux. Since then, however, improvements have been wrought in the efficiency at which slow positrons can be produced from β^+-emitting sources[20] and, more significantly, the concept of "brightness enhancement" proposed by Mills[21] has been implemented.

Brightness enhancement is based on the same non-phase-space-conserving process that is responsible for producing slow positrons with negative work-function moderators that are irradiated with fast positrons from β^+-emitting sources.[20] Slow positrons emitted from the primary moderator are accelerated to a few keV and then focused to a small spot onto another moderator, or remoderator. For a well-prepared single-crystal remoderator, 30–50% of the incident positrons are reemitted as slow positrons.[22,23] The loss in positron flux due to remoderation is insignificant compared to the increase in flux per unit area, or equivalently the brightness,[24] when one considers that the emitting diameter can be decreased by up to a factor of 100 in the process. As described in Sec. II, the high brightness beam at Brandeis University employs two stages of weak focusing reflection mode brightness enhancement,[22,23] which reduces the beam emitting diameter by a factor of 10 in each stage. A variation of the two-stage approach, employed by Frieze, Gidley, and Lynn[25] in the first demonstration of brightness enhancement, achieved a factor of 50 in brightness enhancement. This beam was subsequently used by Mayer *et al.*[26] to repeat the first generation LEPD measurements of Cu(100) by Weiss *et al.*[27] but with improved beam characteristics. The surprising outcome of the measurements was that there was no dramatic improvement in the ability to see fine details in the *I-V* profiles. This result was not due entirely to insufficient brightness enhancement in itself, but also to the fact that Mayer *et al.* were restricted to a large incident polar angle of 53.5° which, due to increased inelastic scattering, led to a smearing out of fine details in their *I-V* profiles.[28] As described in Sec. II, the 500-fold brightness

enhancement achieved at Brandeis University eliminated this problem by enabling normal-incidence LEPD measurements to be performed.

The original impetus for improving LEPD beyond the early experiments came mainly from two realizations: (1) For positrons incident on metals, there are fewer excluded final scattering states than for electrons. This fact results in a shorter elastic mean free path, λ_{ee}, and hence greater surface sensitivity for positrons.[29] (2) Ion core repulsion of the positron greatly reduces the sensitivity of the positron scattering phase shifts to the treatment of positron correlation with core electrons in the I-V profile calculations.[30–32] As pointed out by Read and Lowy,[33] this feature of LEPD would make it ideally suited for high-Z materials where the lack of a first-principles treatment of exchange-correlation effects in electron-ion scattering can limit the accuracy of LEED structural determinations.[34] In addition to the expected improvements in the accuracy of calculated scattering phase shifts employed in a LEPD analysis, it was anticipated that the large differences observed between LEPD and LEED I-V profiles would make LEPD an important compliment to LEED. Structural parameters of binary systems, for example, would be better constrained by requiring that theoretical I-V profiles $I_{\rm th}(V)$ fit both LEED and LEPD experimental profiles $I_{\rm ex}(V)$ since positrons and electrons exhibit differing phase shifts or "contrasts" with respect to the anion and cation of the compound system.[27,32] It was this context, in addition to the importance of the wurtzite CdSe surfaces, that motivated the choice of these surfaces for the first modern LEPD structural determination.

We proceed by discussing the experimental procedures in Sec. II and the calculation of LEPD intensities in Sec. III. The structure analysis is described in Sec. IV for the (10$\bar{1}$0) surface and in Sec. V for the (11$\bar{2}$0) surface. A discussion of these results is provided in Sec. VI, followed by conclusions in Sec. VII.

II. EXPERIMENTAL PROCEDURES

The measurements of LEED intensities were performed by two independent groups, one at Brandeis University and another at Princeton University. We first describe the experimental procedure at Brandeis. The Brandeis apparatus possessed the capability of collecting both LEED and LEPD data from the same sample surfaces, in the same geometry, and by the same detector array. This procedure ensured that both electron and positron data could be compared in an unambiguous manner.

The positron beam utilized slow (~3 eV) positrons produced by β^+ irradiation of a negative affinity W(110) single-crystal moderator[35] by a 230-mCi ^{58}Co radioactive source. The source faced a 9-mm-diam, 2-mm-thick moderator in a backscattering geometry.[24] The source-moderator assembly served as the cathode of an electrostatic extraction gun[36] which injected the slow beam into a transport system for collimation, acceleration, and condensing to a small focus on a second W(110) moderator.[21] The slow positrons remoderated from this <1-mm focus were then extracted and focused to a 100-μm spot on a third moderator, where the extraction and collimation procedure was repeated to produce the final beam. This method of reducing the slow positron emitting diameter allowed us to produce a 1-mm-deg, 25-eV e^+ beam with 500 times greater flux than could be achieved by simply aperturing the unenhanced beam.

For electrons, a thermionic source was a filament located adjacent to the third moderator, which could be retracted *in situ* to allow the thermal electrons to enter the same extraction optics used to collect the slow positrons. The beam (e^- or e^+) was then transported at 1 keV to a standard surface analysis chamber, where it was collimated to a 1-mm-diam, 1° divergence variable-energy beam by an afocal five-element zoom lens.[37] This lens produced a (20–250)-eV beam with nearly constant phase-space characteristics by producing a crossover at the nominal position of the sample. Details of the beam design and performance characteristics have been documented elsewhere.[5,23,38] Incident fluxes of 5×10^3 e^+/s and 4×10^4 e^-/s were determined by means of an electrostatic mirror which could be moved into the sample position to deflect the incoming beam into the diffractometer. Figure 3 displays the transmission properties of the lens system as a function of energy, measured with a position-sensitive detector. The diffractometer, a schematic diagram of which is shown in Fig. 4, consisted of three hemispherical, 80% transmission grids[39] concentric with a position-sensitive detector comprised of a dual-chevron microchannel-plate array[40] (CEMA) and resistive anode encoder (RAE).[41] The 3-in.-diam array allowed an acceptance angle of 100°. In order to minimize the distortions introduced by mapping the diffracted beams passed by the three-grid hemispherical energy analyzer onto the planar CEMA, the diffractometer was operated with an accelerating field between the third grid and CEMA front plate. In addition to increasing the angular acceptance,

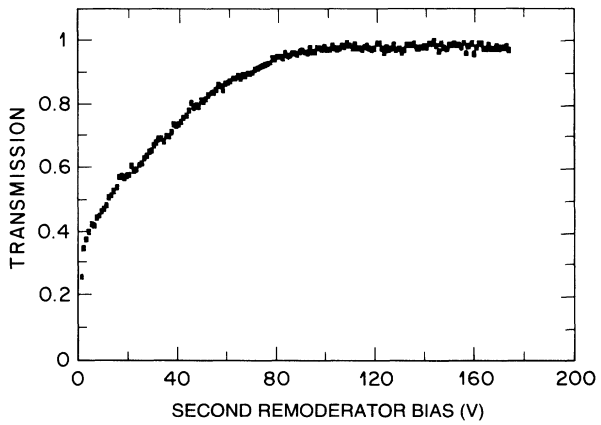

FIG. 3. Measured transmission coefficient of the positron beam as a function of the second remoderator (RM2) bias, monitored at the sample position. The relation between the RM2 bias $V_{\rm RM2}$ and the beam energy E is given by $E = -eV_{\rm RM2} - \phi_+$, where the positron work function $\phi_+ \approx -3$ eV for the W(110) remoderator.

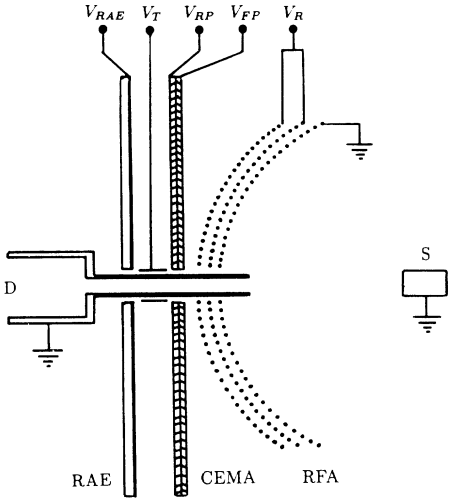

FIG. 4. Diagram of the Brandeis low-energy positron-electron diffractometer. As described in Sec. II, it consists of a resistive anode encoder (RAE), a dual chevron channel electron multiplier array (CEMA), and a three-grid retarding field analyzer (RFA); the final element of an electrostatic zoom lens is denoted by D, and the sample by S. For positrons, the RAE is held at $V_{\mathrm{RAE}} = +1800$ V, the lens shield at $V_T = +1650$ V, CEMA rear plate at $V_{\mathrm{RP}} = +1500$ V, CEMA front plate at $V_{\mathrm{FP}} = -150$ V, and the dual retarding grids at $V_R = V_{\mathrm{RM2}} - 2$ V.

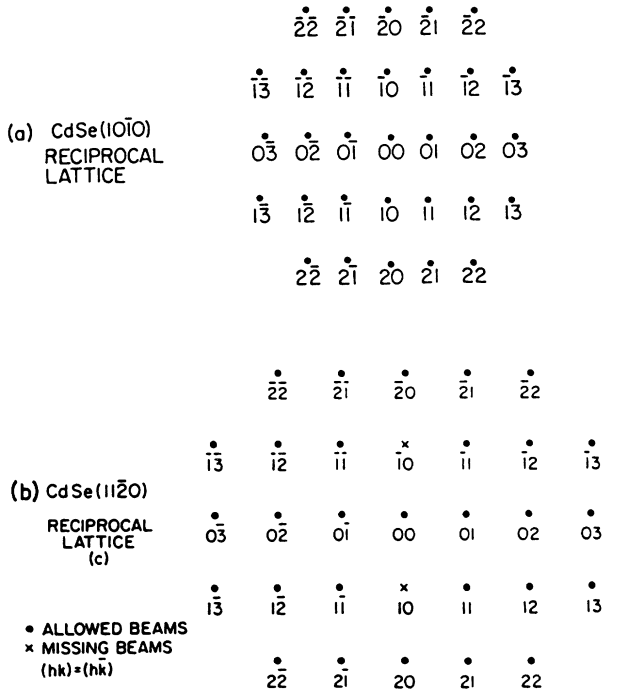

FIG. 5. Normal incidence spot patterns (i.e., reciprocal lattices) of CdSe(10$\bar{1}$0) (a) and CdSe(11$\bar{2}$0) (b).

this feature reduced the effects of the nonlinear response of the CEMA due to variations in incidence angle,[42] α, which we estimate to be $-7° < \alpha < 7°$.

The CdSe(10$\bar{1}$0) and CdSe(11$\bar{2}$0) samples[43] were high-purity, sulfur-free, n-type low-resistivity ($\rho < 10\ \Omega$ cm) single-crystal boules of dimension 5 mm×5 mm×20 mm. They were attached to a thin copper holder with silver epoxy[44] to ensure good thermal and electrical contact, and mounted on a manipulator which provided liquid-nitrogen cooling and five positional degrees of freedom: x, y, z, θ, and Φ. The surfaces were prepared via *in situ* cleaving at $\sim 10^{-10}$ Torr by a specially constructed cleaver[38] which utilized a chisel and anvil design. The surface analysis chamber also contained a display LEED system for monitoring the uniformity of the cleaved surface prior to its positioning in front of the diffractometer. The CdSe samples, after cleaving, were cleaned periodically by heating and the diffracted intensities monitored to ensure that the total 100-h run period required for a complete energy scan corresponded to clean surface conditions in the mid-10^{-11}-Torr sample chamber.

The normal-incidence spot patterns and indexing conventions characteristic of the (10$\bar{1}$0) and (11$\bar{2}$0) two-dimensional (2D) reciprocal lattices are shown in Figs. 5(a) and 5(b), respectively. Both the (10$\bar{1}$0) and (11$\bar{2}$0) directions are normal to the (0001) or c axis, and are rotated 90° from one another. Thus, the unit vectors along these three directions are mutually orthogonal. The c axis defines both a mirror plane of the (10$\bar{1}$0) surface net and a glide plane of the (11$\bar{2}$0) surface net. Thus for incidence angles having no projection transverse to the c axis, all beams not along (0001) are twofold degenerate.

The beam energy and data-collection instrumentation were under computer control. The beam energy was ramped in 2-eV increments with a dwell time of 100 s. A digital record of the diffraction pattern and absolute intensities were recorded at each energy point, and stored as a 256×256 channel ×16 bit deep histogram. Prior to recording the next point, the data were binned by 4 and stored in a 64×64 segment of a 256×256 matrix, allowing images at 16 consecutive energy points to be stored in a single 64 K file. The file was displayed on a graphics terminal via interactive software[45] and updated after each dwell cycle. Once 16 images were obtained, the beam energy was reset to its starting value and the 30-eV range scan repeated, creating a new file consisting of the sum of the two scans. This "multiscaling" was continued until statistically reliable data sets were obtained, requiring between 20 and 40 scans for LEPD and 3–4 scans for LEED. Some overlap was provided between adjacent energy ranges, requiring six separate multiscaled files to generate data from 20 to 160 eV. Collection times were typically 3 days for LEPD and 6 h for LEED. Diffracted intensity versus energy (I-V) curves were generated by manually defining a region of interest (ROI) via the interactive graphics software and recording both the integrated counts within an ROI enclosing a particular beam and the background counts adjacent to that beam. This procedure was repeated for each of the (~20) beams subtended by the diffractometer. Subsequent to background subtraction, the I-V curves were converted to absolute reflectivities by dividing by an incident beam

I-V measured via the electrostatic mirror prior to beginning the data collection. The symmetry-equivalent beams [(hk)=$(-hk)$ for (10$\bar{1}$0) and $(hk) = (h-k)$ for (11$\bar{2}$0)] were then averaged to produce the final experimental I-V curves.

Equivalent beam averaging (EBA) has been shown to reduce the effects of systematic errors due to stray magnetic fields and sample misalignment.[46] Although homogeneous magnetic fields within the sample interaction region were carefully nulled by the use of large-diameter Helmholtz coils,[37] we observed a drift in incident polar angle which resulted in a purely horizontal displacement of 1.5 mm across the sample face as the beam energy was increased from 20 to 160 eV. As expected, the electron beam displayed a similar drift, but opposite to that of the positron beam. By calibrating the motion of beams across the diffractometer as a function of incidence angle, we estimated the total drift to be $\delta\theta < 2°$ between 20 and 160 eV. Since there was no observed drift in the azimuthal angle Φ, it was possible to position the sample such that the (0001) or symmetry axis was oriented vertically, forcing any drifts in polar angle θ to break the symmetry of equivalent beams. In this manner we not only generated a useful diagnostic for variations in θ, but also maximized the utility of the EBA procedure. Only small differences were observed, however, in the absolute intensities of equivalent pairs. Figure 6 illustrates the EBA procedure using the {$\bar{1}$1} beams from CdSe(11$\bar{2}$0). It can be seen that the symmetry-equivalent profiles are indeed equivalent within statistical uncertainties.

During the course of the experiments, duplicate data sets were collected from surfaces resulting from different

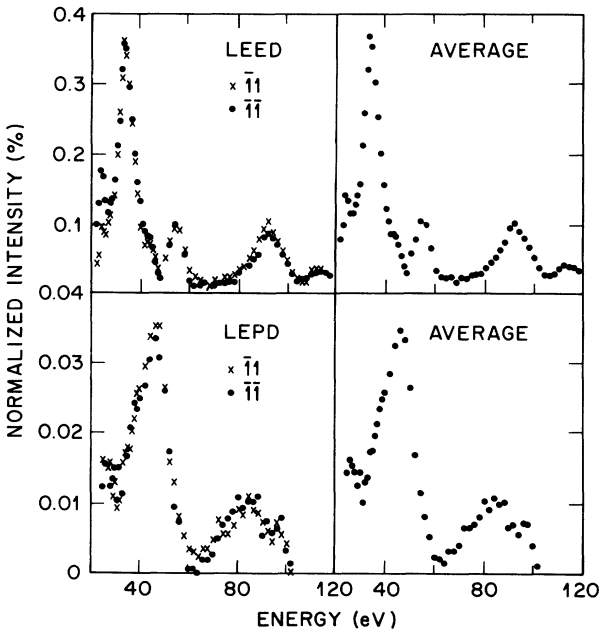

FIG. 6. Comparison of the equivalent ($\bar{1}$1) and ($\bar{1}\bar{1}$) diffracted beams from CdSe(11$\bar{2}$0) averaged to obtain the data used in comparison with theoretical calculations. LEED intensities are shown in the upper panel and LEPD intensities in the lower panel.

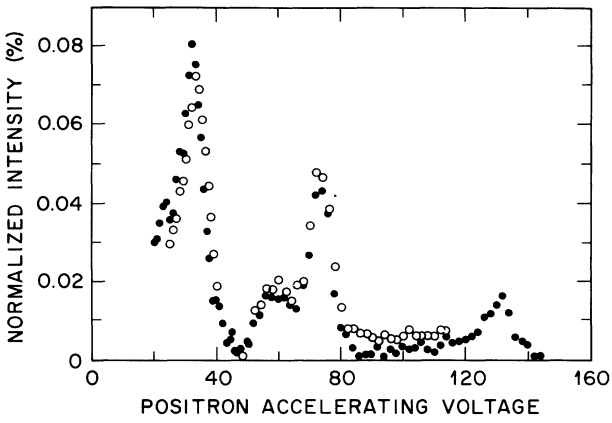

FIG. 7. Comparison of the (22) LEPD beams obtained from two separate CdSe(11$\bar{2}$0) cleaves. Solid circles: cleave 1. Open circles: cleave 2. Accelerating voltage is in units of volts.

cleaves, both from the (11$\bar{2}$0) and (10$\bar{1}$0) sample boules. I-V profiles were obtained from different cleaved surfaces in order to document the reproducibility of the surface preparation. One such I-V pair resulting from two consecutive cleaves is displayed in Fig. 7. The fact that the two data sets agree well both in absolute reflectivities and peak positions indicates that reproducibly uniform surfaces were prepared, as was also evidenced by sharp (1×1) LEED patterns. Similar results were obtained from both the (10$\bar{1}$0) and (11$\bar{2}$0) cleavage faces.

The Princeton LEED I-V profiles from similarly prepared CdSe samples[11] were obtained from 20 to 240 eV using a spot photometer. In this case, symmetry equivalence was checked for several pairs of beams at various energies, but the equivalent beams were not averaged. Instead, three complete sets of I-V profiles were collected and then averaged. Normalization was accomplished by monitoring the current leaving the electron gun.

The LEPD data were collected at an angle of incidence of $\theta = 3.5°, \Phi = \pi/2$ for CdSe(10$\bar{1}$0) and $\theta = 1.8°, \Phi = \pi$ for CdSe(11$\bar{2}$0). The Brandeis LEED data were collected at an angle of incidence of $\theta = 1.5°, \Phi = \pi/2$ for CdSe(10$\bar{1}$0) and $\theta = \Phi = 0$ for CdSe(11$\bar{2}$0). $\Phi = 0$ is defined along the $\mathbf{a}_x$ real-space lattice vector of the surface net as indicated in Figs. 1 and 2; the $\pi/2$ discrepancy in Φ between the two surfaces is a consequence of the crystallographic convention which assigns $\mathbf{a}_x$ to be parallel to the smaller of the two primitive lattice vectors of the unit cell.

Ten (twelve) beams comprised the LEPD (LEED) data for (10$\bar{1}$0) while fourteen (thirteen) beams comprised the LEPD (LEED) data for (11$\bar{2}$0). For LEED from CdSe(10$\bar{1}$0), these were the (01), (0$\bar{1}$), (10)=($\bar{1}$0), (11)=($\bar{1}$1), (1$\bar{1}$)=($\bar{1}\bar{1}$), (02), (0$\bar{2}$), (20)=($\bar{2}$0), ($\bar{1}$2)=(12), ($\bar{1}\bar{2}$)=(1$\bar{2}$), (03), and (0$\bar{3}$) which exhibited the expected $(hk) = (-hk)$ symmetry. For CdSe(11$\bar{2}$0), these were the (01)=(0$\bar{1}$), (11)=(1$\bar{1}$), ($\bar{1}$1)=($\bar{1}\bar{1}$), (20), ($\bar{2}$0), (02)=(0$\bar{2}$), (12)=(1$\bar{2}$), ($\bar{1}$2)=($\bar{1}\bar{2}$), (21)=(2$\bar{1}$), ($\bar{2}$1)=($\bar{2}\bar{1}$), (03)=(0$\bar{3}$), (13)=(1$\bar{3}$), and ($\bar{1}$3)=($\bar{1}\bar{3}$) which exhibited the expected (hk)=$(h-k)$ symmetry and missing $(h0)$ beams for

odd values of h. For LEPD from CdSe(10$\bar{1}$0), the (20) and (1$\bar{2}$) beams were not recorded. For LEPD from CdSe(11$\bar{2}$0), the (22)=(2$\bar{2}$), ($\bar{2}$2)=($\bar{2}\bar{2}$), (31)=(3$\bar{1}$), ($\bar{3}$1)=($\bar{3}\bar{1}$), and (23)=(2$\bar{3}$) beams were added and the (21), ($\bar{2}$1), (13), and ($\bar{1}$3) beams were not measured. The initial LEPD intensities for CdSe(10$\bar{1}$0) were obtained for a room-temperature sample. All others were measured with the sample cooled to 105< T <120 K by pumping dry nitrogen through a heat exchanger immersed in a liquid-nitrogen reservoir and through the sample mount.

III. INTENSITY CALCULATIONS

Our calculation of both the LEED and LEPD intensities has been described in considerable detail by Weiss *et al.*[27] for Cu(100) and Cu(111). Therefore in this section we review the model and calculational procedure only briefly, considering those aspects required for the definition of the model and the discussion in Sec. VI of the differences between LEED and LEPD.

The construction of the electron-ion core potential used to generate the phase shifts needed as input parameters for the LEED and LEPD intensity calculation has been specified for CdSe by Duke and Lessor,[32] hereafter referred to as DL. Each ion core is represented by a spherical potential, $V(r)$, given by

$$V(r) = V_a + V_{\text{exch}} \tag{1}$$

in which for electrons

$$V_a = \frac{-Ze^2}{|r|} + e^2 \int d^3r' \, \frac{\rho(r')}{|r - r'|} \tag{2}$$

is obtained from the self-consistent charge density, $\rho(r)$ around the ion core. In our calculations the $\rho(r)$ are obtained from self-consistent solutions to the Dirac equation using a computer program due to Liberman and coworkers[47,48] For positrons the same procedure is utilized with the one change that the signs of both terms on the right-hand side of Eq. (2) are reversed.

The exchange contribution to the potential, V_{exch} in Eq. (1), is nonvanishing only for electrons. In calculations of the ground-state charge density a local form, typically Slater[49] or Kohn-Sham[50] is used. For the higher-energy electrons used in LEED an energy-dependent Hara[51] exchange potential is utilized as described by Meyer, Duke, and Paton.[52]

Once the atomic potentials have been defined as indicated above, the crystal potentials are obtained by superimposing the atomic potentials and reducing the resulting superposition to muffin-tin form as described by Ford, Duke, and Paton.[53] Evidentially, the muffin-tin radii are different for electrons and positrons because the former embody the extra (attractive) exchange terms. Since, moreover, these terms are energy dependent, the muffin-tin radii for electrons also depend slightly on the electrons' energy. Examples of these potentials are shown in Fig. 1 of DL.

Once the muffin-tin potential is defined, energy-dependent phase shifts are obtained by solving the nonrelativistic radial Schrödinger equation:

$$\left[\frac{\hbar^2}{2m}\frac{d^2}{dr^2} + E - qV(r) - \frac{\hbar^2 l(l+1)}{2mr^2}\right]\Psi_l(r) = 0, \tag{3}$$

where Ψ_l is matched to its asymptotic form at the muffin-tin radius. E is the energy of the particle relative to the muffin-tin zero and q is $+e$ for positrons and $-e$ for electrons. The resulting phase shifts are shown as a function of E for both positrons and electrons in Figs. 2 and 3, respectively, of DL. The LEED phase shifts differ slightly from those used in an earlier analysis[11] of CdSe(10$\bar{1}$0) because of a correction which was required in the calculation of the Hara exchange potential.[54]

In order to account for lattice vibrations, the phase shifts incorporated an imaginary part characterized by rms displacements of the vibrating lattice.[55] In the CdSe(10$\bar{1}$0) analysis, we use the same values of these $\langle u^2 \rangle$ as Duke *et al.*,[11] namely $\langle u^2 \rangle$(Cd)=0.090 Å^2 and $\langle u^2 \rangle$(Se)=0.075 Å^2. These values are roughly three times what one would expect from estimates of the bulk Debye temperature for CdSe.[56,57] In contrast, best agreement was found with the CdSe(11$\bar{2}$0) data (both electrons and positrons) by using rigid-lattice phase shifts (i.e., $\langle u^2 \rangle = 0$).

In addition to the ion-core phase shifts, a complex inner potential, $\Sigma(E)$, describing the propagation of the incident electron or positron through the interacting electron fluid in between the muffin-tin spheres must be specified. For electrons we utilize the form[58]

$$\Sigma(E) = -V_0 + \frac{-i\hbar[2m(E+V_0)]^{1/2}}{m\lambda_{ee}}, \tag{4}$$

where λ_{ee} is the inelastic-collision damping length. This form of the inner potential describes a particle whose mean free path is constant, $\lambda = \lambda_{ee}/2$. For electrons, λ_{ee} is set to 10 Å, in correspondence with a previous LEED analysis of CdSe(10$\bar{1}$0).[11]

For positrons, the following expression[27] is used:

$$\Sigma(E) = -V_0 - iV_i, \tag{5}$$

where V_i is a constant. The value for V_i is chosen as 4.65 eV based upon a search in V_i to best represent agreement with the measured diffraction intensities. Both the form for Σ and the value of V_i are consistent with previous LEPD analyses.[27,28,31]

The values of V_0 are obtained by comparison of the measured and calculated values of the intensities in the vicinity of the best-fit structures.[11] This procedure yields $V_0 = 2 \pm 1$ eV for LEPD and $V_0 = 12 \pm 2$ eV for LEED.

A multiple-scattering model of the electron and positron diffraction process, described previously,[59] is used to perform the dynamical calculations of the LEED and LEPD intensities for given surface atomic geometries. In this model, the scattering species are represented by the energy-dependent phase shifts whose calculation is described above. Each atomic layer parallel to the surface is divided into one (two) Cd and one (two) Se primitive sublattices of symmetry-equivalent scatterers parallel to the CdSe(10$\bar{1}$0) [(11$\bar{2}$0)] surface. The two Cd and Se sublattices for CdSe(11$\bar{2}$0) can be shown to be symmetry equivalent for an unrelaxed surface, but for various re-

laxed geometries, the equivalence must be verified explicitly via the multiple scattering calculations *per se*.[60] Each two-dimensional surface unit cell includes one atom from each of the primitive sublattices (Figs. 1 and 2). The scattering amplitudes for each sublattice are evaluated analytically, whereas the scattering between sublattices is described by a set of coupled matrix equations expressed in the angular momentum representation.[61] These equations are solved "exactly" for a prescribed number of the top layers which is varied until convergence is achieved. For deeper layers, the scattering amplitudes for each layer are obtained by considering the multiple scattering between the two (four) sublattices within the layer but neglecting the multiple scattering between layers. The LEED and LEPD intensities are expressed as a superposition of the scattering amplitudes for the individual layers calculated as indicated above.[58,59,61] Fourteen atomic layers of scatterers are included in the calculation.

In general, treating the scattering exactly within the top three [CdSe(11$\bar{2}$0)] or four [CdSe(10$\bar{1}$0)] bilayers suffices to perform the structural search, i.e., to give a 2% convergence of the intensity line shapes. The intensities associated with the final "best-fit" structure were recalculated with the scattering from the top six layers evaluated exactly for CdSe(10$\bar{1}$0) and the top four exactly for CdSe(11$\bar{2}$0), resulting in only slightly improved agreement between the calculated and measured intensities.

The resulting diffraction intensities for the individual (hk) beams are output as a file containing absolute reflectivities as a function of incident energy, in 2-eV increments. These are compared with measured LEED and LEPD intensities to determine the positions of the scatterers in the surface region of the sample. The fit between experimental and calculated intensity versus energy profiles is quantified by using R_X the x-ray R factor,[62] and R_I the integrated intensity R factor.[63] The latter gives a measure of how well the calculation accounts for the relative strength of various beams. For each calculation, V_0 was selected to minimize R_X. The manner in which R_X provides a measure of agreement between the theoretical and experimental I-V profiles can be seen in the following equations:

$$R_X = \left(\frac{3}{2n} + \frac{2}{3}\right) r \ , \tag{6}$$

$$r = \sum_i r_i (E_{fi} - E_{si}) \Big/ \sum_i (E_{fi} - E_{si}) \ , \tag{7}$$

$$r_i = \sum_E [C_i \, I_{\rm th}^{(i)}(E) - I_{\rm expt}^{(i)}(E)]^2 \Big/ \sum_E [I_{\rm expt}^{(i)}(E)]^2 \ , \tag{8}$$

where C_i is determined from the condition

$$\frac{\partial r_i}{\partial C_i} = 0 \ . \tag{9}$$

The index i represents each of the n diffracted beams; E_{fi} and E_{si} are the final and beginning energy end points, respectively, for the ith beam I-V profile. R_I is defined by

$$R_I = \sum_i [(A_{\rm th}^{(i)} - A_{\rm expt}^{(i)})/A_{\rm expt}^{(i)}]^2 \ , \tag{10}$$

where

$$A^{(i)} = \sum_E I^{(i)}(E) \tag{11}$$

for both theoretical and experimental I-V profiles, and the profiles have been normalized to each other for the strongest diffracted beam.

IV. STRUCTURE ANALYSIS: CdSe(10$\bar{1}$0)

The CdSe(10$\bar{1}$0) surface consists of isolated Cd-Se dimers in which each atom exhibits one surface and two back (or subsurface) bonds, as illustrated in Fig. 1. The surface unit cell is rectangular, where the two primitive lattice vectors $\mathbf{a}_x$ and $\mathbf{a}_y$ are indicated in Fig. 1(b). This surface relaxation model is substantially identical to that which originally was developed for zinc-blende (110) surfaces,[2,3] i.e., a bond-length-conserving rotation of the Cd-Se surface dimer. For CdSe(10$\bar{1}$0) each surface atom has one surface nearest neighbor and two substrate neighbors, whereas for zinc-blende (110) each surface species has two surface nearest neighbors and only a single-substrate nearest neighbor. This model was extended to include wurtzite-structure compound semiconductors by Duke *et al.*,[11] who successfully applied it to the analysis of the CdSe(10$\bar{1}$0) surface. Our analysis follows theirs. Brief accounts of it have been given already.[5,6]

Four independent surface structural parameters are defined in Fig. 1. The first of these is the dimer rotation angle ω. The others are the vector shear between the Cd and Se in the first two layers, Δ_1 and Δ_2, and the first interlayer spacing d_{12}. The vector shear has two independent variable components: one normal to the surface, $\Delta_{i,\perp}(i = 1, 2)$, and one along the y [or (0001)] axis, $\Delta_{i,y}$. The observed mirror symmetry of the diffracted intensities requires that $\Delta_{i,x}$ equal its bulk value, i.e., $\Delta_{i,x} = a_x/2$. The first interlayer spacing d_{12} likewise has two variable components, $d_{12,\perp}$ and $d_{12,y}$. The initial structural search was conducted by linking the values of $\Delta_{i,\perp}$, $\Delta_{i,y}$, $d_{12,\perp}$, and $d_{12,y}$ such that all the bond lengths remain constant as ω is varied. The components of the first-layer shear are given by

$$\Delta_{1,\perp} = d \sin \omega, \tag{12}$$

$$\Delta_{1,y} = a_y - d \cos \omega, \tag{13}$$

where $d = 2.63$ Å is the top-layer Cd-Se bond length, and $a_y = 7.02$ Å is the magnitude of the longer primitive lattice vector of the surface unit cell. The condition of constant bond lengths also generate changes in $d_{12,\perp}$ and $d_{12,y}$ as ω is varied.[5]

The structural search was initiated by varying ω over the range $0° \leq \omega \leq 30°$. The resulting values of R_X and R_I are shown in Figs. 8 and 9, respectively. The minima in R_X are used to determine initial values of ω, (ω_0), for the subsequent search. This procedure yields ω_0(LEED)=21° and ω_0(LEPD)=15°, although the min-

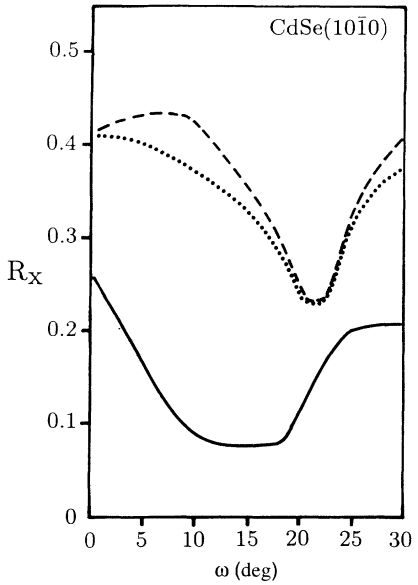

FIG. 8. Variations in the LEED and LEPD x-ray R factors associated with bond-length-conserving rotations ω of the top-layer dimers for CdSe(10$\bar{1}$0). Solid line: LEPD. Dotted line: Brandeis LEED. Dashed line: Princeton LEED.

imum in R_X for LEPD is very flat.

Once ω is roughly determined, i.e., $\omega \sim \omega_0$, the nonstructural parameters V_0, V_i, and λ_{ee} were optimized to give the lowest value of R_X. Convergence tests were then performed, whereby the number of layers treated exactly was incremented and the changes in both intensity line shapes and R_X noted. It was in this manner that treating the scattering from the top four layers exactly was found adequate for the structural search, while an exact treatment of six layers was needed for absolute convergence. The LEPD calculations required treatment of the scattering exactly in approximately one fewer layer to achieve the same degree of convergence as the LEED calculations due to the shorter positron inelastic collision mean free path. This effect was neglected, however, and the same number of exact layers was used in each case.

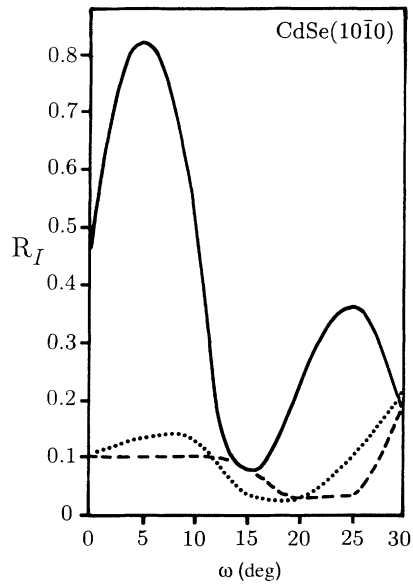

FIG. 9. Variations in the LEED and LEPD integrated intensity R factors associated with bond-length-conserving rotations ω of the top-layer dimers for CdSe(10$\bar{1}$0). Solid line: LEPD. Dotted line: Brandeis LEED. Dashed line: Princeton LEED.

With the nonstructural parameters thus optimized, the minima in the $R_X(\omega)$ plots were defined in great detail by varying ω in 1° increments about the previously defined coarse minima. The "optimum" value of ω was determined as the centroid of this roughly parabolic minimum. In the case of the LEPD determination of CdSe(10$\bar{1}$0), $\omega(R_X) = 15°$. In the LEED determination of CdSe(10$\bar{1}$0), $\omega(R_X) = 21.5°$.

In general, R_X and R_I do not converge at the same value of ω just as in the case of zinc-blende-structure materials.[2] The origin of this fact lies in the extreme sensitivity of R_I to the precise energy range of the data set, a fact which leads us to use it to discriminate between roughly equivalent minima in R_X but not as a primary structural indicator.[63] With ω thus optimized, contractions of the first interlayer spacing were explored by varying $d_{12,\perp}$, followed by considering counterrotations of the second layer via refinements to the value of $\Delta_{2,\perp}$. Relaxations parallel to the surface were not examined in detail after preliminary searches in these variables failed to improve the fits to the data for variations of ±0.2 Å. The final best-fit structures are indicated in Table I along with the results associated with the predicted[17,64] structure for CdSe(10$\bar{1}$0). Comparisons between the predicted and measured intensities of strong beams are shown in Figs. 10 and 11 for LEED and LEPD, respectively.

In order to estimate the uncertainties inherent in the structural analysis, the criterion utilized in earlier studies of zinc-blende (110) surfaces[65] was employed. This criterion consists of assigning limits to the sensitivities of R_X in discriminating between two possible structures. While a change of 0.02 in R_X is considered significant, a change of 0.04 is sufficient to absolutely discriminate between two structures. Since the relaxations of the secondary parameters $d_{12,\perp}$ and $\Delta_{2,\perp}$ are admittedly of the order of their uncertainty, we do not attempt to utilize this method of error assignment to those variables. Referring to Fig. 8, one varies R_X about its minimum to establish the change in ω, $\sigma(\omega)$, induced by a "significant" change in R_X:

$$\sigma(\omega) \approx |\omega_{(R_{\min}+0.04)} - \omega_{(R_{\min})}| \, . \tag{14}$$

Utilizing this method of assigning uncertainties to ω, we obtain

$$\text{LEPD: } \omega = 15° \pm 5°, \tag{15}$$

$$\text{LEED: } \omega = 21.5° \pm 3°. \tag{16}$$

For the results of the secondary structural search (with nominal error estimates), we have

$$\text{LEPD: } \delta d_{12,\perp} = -0.10 \pm 0.05 \text{ Å} \, , \tag{17}$$

TABLE I. Structural parameters and associated R factors as determined by (a) LEPD and (b) LEED for the CdSe(10$\bar{1}$0) surface. The results for three structural models are shown: unreconstructed (bulk-terminated), best fit (via R-factor minimization), and theory [predicted in Wang *et al.* (Ref. 64)]. Distances are measured in angstroms; ω is measured in degrees; R_X and R_I are dimensionless.

	$\Delta_{1,\perp}$	$\Delta_{1,y}$	$d_{12,\perp}$	$d_{12,y}$	$\Delta_{2,\perp}$	ω	R_X	R_I
				(a) LEPD				
Unreconstructed	0	4.39	1.24	3.51	0	0	0.23	0.52
Best fit	0.68	4.48	0.65	3.96	−0.05	15°	0.08	0.05
Theory	0.75	4.57	0.68	3.99	−0.05	17°	0.11	0.03
				(b) LEED				
Unreconstructed	0	4.39	1.24	3.51	0	0	0.39	0.21
Best fit Brandeis	0.96	4.57	0.45	4.07	0	21.5°	0.19	0.05
Best fit Princeton	0.96	4.57	0.45	4.07	0	21.5°	0.21	0.03
Theory	0.75	4.57	0.68	3.99	−0.05	17°	0.33	0.07

$$\Delta_{2,\perp} = -0.05 \pm 0.05 \text{ Å} ; \quad (18)$$

$$\text{LEED: } \delta d_{12,\perp} = -0.025 \pm 0.05 \text{ Å} , \quad (19)$$

$$\Delta_{2,\perp} = 0 \pm 0.05 \text{ Å} , \quad (20)$$

where the departure of $d_{12,\perp}$ from its purely bond-length-conserving value is denoted by $\delta d_{12,\perp}$. The structural search reported herein did not include a study of variations in the lateral displacements, i.e., in $d_{12,y}$ or $\Delta_{1,y}$. Since the reported sensitivity of LEED determinations of lateral displacements is on the order of ±0.2 Å,[2,3] we did not consider a precise determination of such variations to be useful.

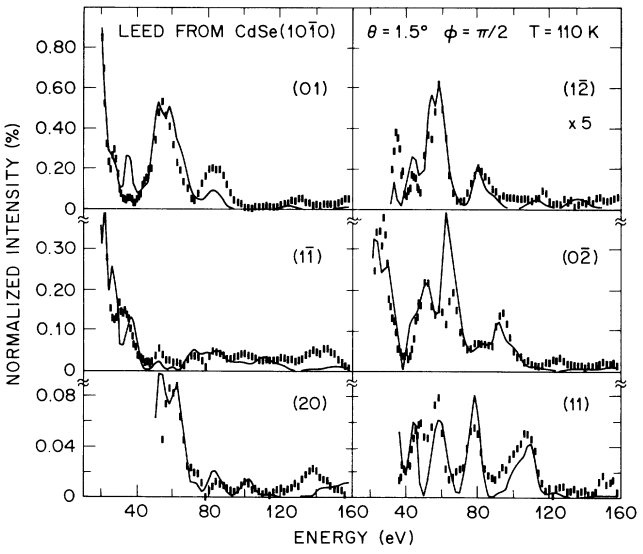

FIG. 10. Comparison of calculated and measured LEED intensities from CdSe(10$\bar{1}$0). The (01) beam is representative of the strong beams [(0$\bar{1}$), (10), and (01)]; the (1$\bar{1}$) and (0$\bar{2}$) of the moderate intensity beams [(0,$\bar{2}$), (02), (1$\bar{1}$)], and the (20), (11), and (1$\bar{2}$) of the weak beams [(12), (11), (0$\bar{3}$), (03), (1$\bar{2}$), and (20)]. The sample was held at a temperature of 110 K.

V. STRUCTURE ANALYSIS: CdSe(11$\bar{2}$0)

A remarkable feature of the cleavage surfaces of tetrahedrally coordinated compound semiconductors is the fact that large relaxations of their atomic geometries can occur without the distortion of any bond lengths from their bulk values. For zinc-blende- (110) and wurtzite-(10$\bar{1}$0) structure surfaces, these relaxations may be characterized as rigid rotations of the plane of the surface layer described by a single angular parameter ω giving the tilt between the relaxed and truncated bulk surfaces as described in the preceding section for CdSe(10$\bar{1}$0). For

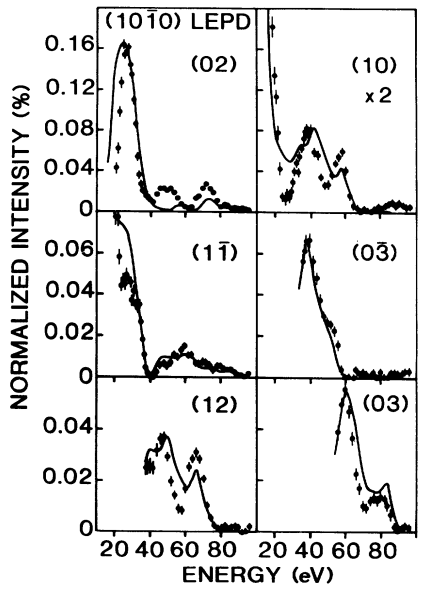

FIG. 11. Comparison of calculated and measured LEPD intensities from CdSe(10$\bar{1}$0). The (02) beam is representative of the strong beams [(02), (0$\bar{1}$), and (0$\bar{2}$)]. The (1$\bar{1}$), (10), (12), and (0$\bar{3}$) beams are all of the moderate-intensity beams. The (03) beam is representative of the weak beams [(01), (11), and (03)]. The sample was held at a temperature of 300 K.

the wurtzite-structure $(11\bar{2}0)$ surface the relaxations are more complicated, however, involving a puckering of the surface layer with the anion relaxing outward and the anion inward. Two angular variables characterize these relaxations, e.g., the angle ω_C between local anion-cation-anion planes and the surface normal and that between local cation-anion-cation planes and the surface normal, ω_A. To achieve a single-variable initial analysis, we select one of these, $\omega = \omega_C$, as the independent variable and use an empirical constitutive relation to relate ω_A to ω based on total-energy calculations.[17,60,64] Hence, the specification of ω defines the structural parameters for bond-length-conserving relaxations. The relation between ω and $\Delta_{1\perp}$, the shear perpendicular to the surface between Cd and Se in the top layer, $\Delta_{1\parallel}$, the relative displacement between Cd and Se parallel to the surface plane, and $d_{12,\perp}$, the distance perpendicular to the surface between the top Cd and the second layer Se (all defined in Fig. 2) is considerably more complex on this surface than on the zinc-blende- (110) or wurtzite- $(10\bar{1}0)$ structure surfaces, and cannot be presented in compact form. A detailed calculation of the x, y, and z coordinates of each surface atom as a function of ω is presented in Appendix B of Kahn, Duke, and Wang.[60] The bond-length-conserving relaxations induce a puckering of the surface unit cell, as indicated in Fig. 2. Unlike the CdSe$(10\bar{1}0)$ surfaces, for which the observed $I(hk) = I(-hk)$ symmetry indicates that surface atomic relaxations are confined to the (y, z) plane, for the CdSe$(11\bar{2}0)$ surface the glide plane symmetry permits arbitrary displacements of the one independent pair of Cd and Se species in the unit cell. The resulting local structure of the surface anion-cation-anion triplets is analogous to that obtained on the $(10\bar{1}0)$ surface.

The initial stage of the structure search consisted of minimizing R_X with respect to ω. LEED and LEPD intensities were calculated for a range of bond-length-conserving relaxations described by $0° \leq \omega \leq 45°$ in steps of 5° for most of the range, and 2° steps near the R-factor minima. The initial scans over ω were conducted using constant values of the inelastic mean free path of 10 and 8 Å for electrons and positrons, respectively. Two R_X minima were found for LEPD: $R_X = 0.22$ for $\omega = 10°$ and $R_X = 0.17$ for $\omega = 27°$. For LEED, two minima also were found: one with $R_X \sim 0.4$ for $\omega = 0$, and another near $\omega = 33°$ with $R_X \sim 0.3$. In addition, the values of R_I are lower for the $\omega \sim 30°$ structure, so we can be

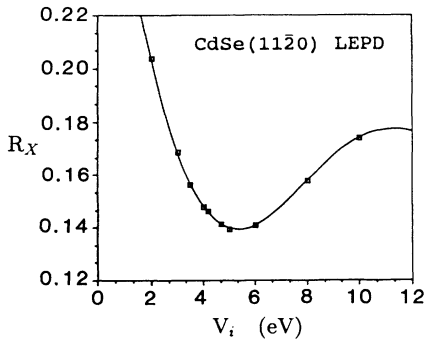

FIG. 12. Variation in the x-ray R factor with the non-structural parameter V_i, the imaginary part of the inner potential. This optimization was performed for the $(11\bar{2}0)$ surface, assuming the following values for the primary structural variables: $\omega = 24°$, $\delta d_{12,\perp} = -0.06$ Å.

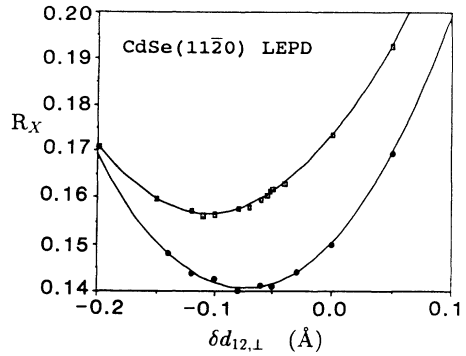

FIG. 13. Variation in the x-ray R factor for the $(11\bar{2}0)$ surface with the structural parameter $\delta d_{12,\perp}$, which denotes the departure from a purely bond-length-conserving relaxation of the first interlayer spacing, $d_{12,\perp}$. The open squares (upper curve) were calculated assuming a constant value of the inelastic mean free path $\lambda_{ee} = 8$ Å. The solid circles (lower curve) were calculated assuming an energy-dependent form of λ_{ee} denoted by a value of $V_i = 4.65$ eV, derived from Fig. 12. The plot was obtained with a bond-rotation angle of $\omega = 24°$.

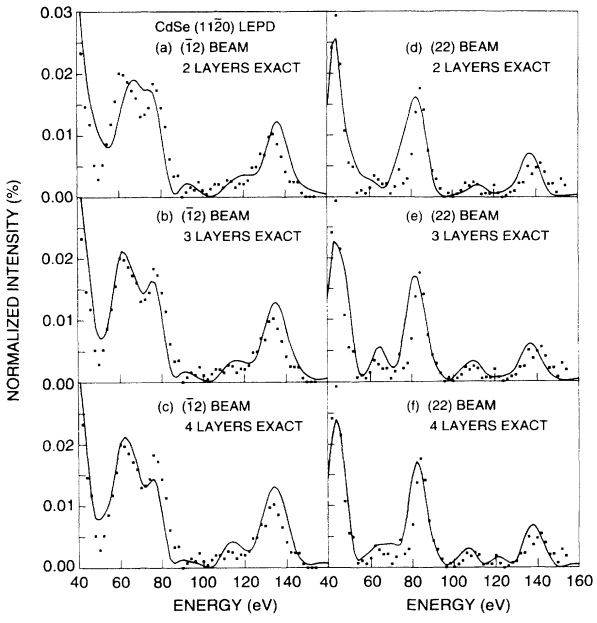

FIG. 14. Convergence tests using the LEPD $(\bar{1}2)=(\bar{1}\bar{2})$ and $(22)=(2\bar{2})$ beams from the CdSe$(11\bar{2}0)$ surface. The number of topmost bilayers treated in a full multiple scattering formalism (i.e., treated "exactly") was varied, as described in the text. Points are measured data, while the solid lines denote diffraction intensities calculated using: (a),(d) two layers treated exactly; (b),(e) three layers treated exactly; (c),(f) four layers treated exactly. Extension of the exact treatment to deeper layers did not substantively improve convergence of the intensity line shapes.

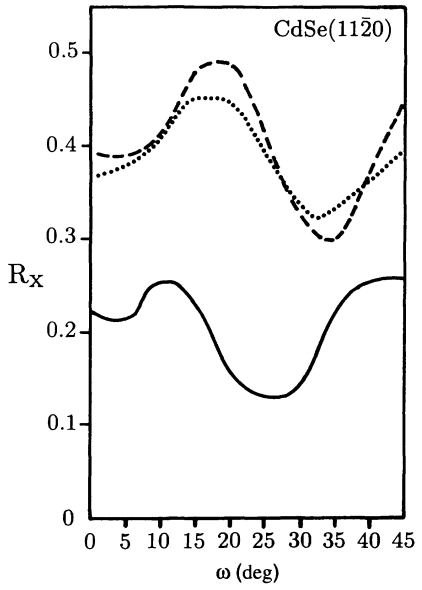

FIG. 15. Variations in the LEED and LEPD x-ray R factors associated with bond-length-conserving relaxations of the top layer (denoted by ω) for CdSe(11$\bar{2}$0). Solid line: LEPD. Dotted line: Brandeis LEED. Dashed line: Princeton LEED.

confident that the surface is relaxed.

The relaxed structures were used as the starting point for further refinements. The first-to-second layer spacing, characterized by $d_{12,\perp}$, was varied within the range $-0.20 \leq \delta d_{12,\perp} \leq 0.08$ Å in the LEPD analysis. This yielded a broad minimum in R_X with a value of 0.16 in the vicinity of $\delta d_{12,\perp} = -0.10$ Å. At this point in the analysis, the form of the complex inner potential was explored. As previously discussed, it has been shown[29] that the adoption of a constant imaginary part of the inner potential, V_i, is a more appropriate choice in the treatment of positron diffraction than the form expressed by Eq. (3.4) which utilizes a constant mean free path. The former describes a particle whose mean penetration depth varies as $E^{1/2}$. Utilizing the initial best-fit structure, the value of V_i was varied over the range $0 \leq V_i \leq 10$ eV and plotted versus R_X, as illustrated in Fig. 12. The best-fit value of $V_i = 4.65$ eV was then incorporated into a reoptimization of the value of $d_{12,\perp}$ to assess the effects of the choice of nonstructural parameters on the final structure. The choice of "best-fit" structure was only slightly affected; however, the quality of the fits were improved, resulting in a decrease in the value of R_X from 0.16 to 0.14. The scans over $\delta d_{12,\perp}$ incorporating each of the two forms of inner potential are illustrated in Fig. 13. It is evident that although the quality of the fits are different, the shape of the R_X versus $\delta d_{12,\perp}$ curves are very similar.

Subsequent to the refinements associated with the incorporation of an energy-dependent inner potential, convergence tests were performed whereby the number of bilayers in which positron scattering is treated "exactly," including both intralayer and interlayer multiple scattering effects, was systematically incremented until a convergence of the intensity line shapes was attained. This procedure is illustrated in Fig. 14 for the ($\bar{1}$2)=($\bar{1}\bar{2}$) and

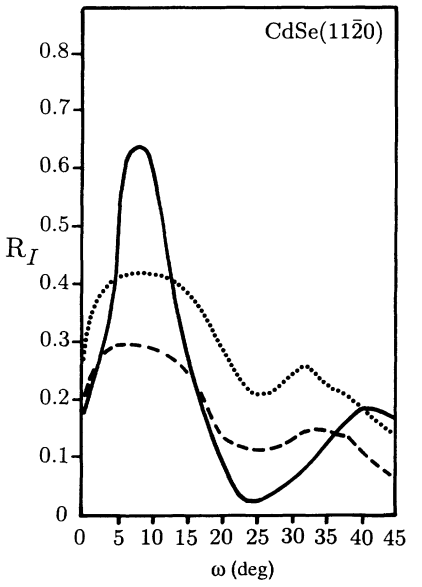

FIG. 16. Variations in the LEED and LEPD integrated intensity R factors associated with bond-length-conserving relaxations of the top layer (denoted by ω) for CdSe(11$\bar{2}$0). Solid line: LEPD. Dotted line: Brandeis LEED. Dashed line: Princeton LEED.

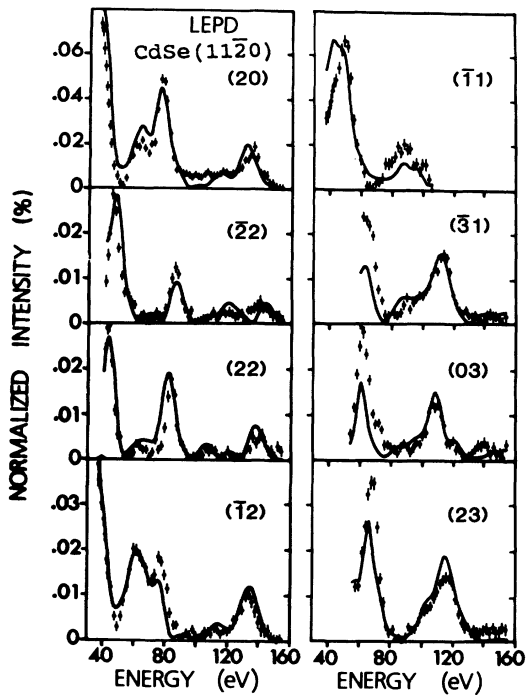

FIG. 17. Comparison of calculated and measured LEPD intensities from CdSe(11$\bar{2}$0). The (20), ($\bar{1}$2), and (23) beams are representative of the strong beams [(20), ($\bar{2}$0), ($\bar{1}$2), and (23)]; the ($\bar{1}$1), ($\bar{3}$1), (03), and ($\bar{2}$2) beams are the moderate intensity beams; the (22) beam is the strongest of the weak beams [(22), (11), (12), (02), (31), and (01)]. The sample was held at a temperature of 110 K.

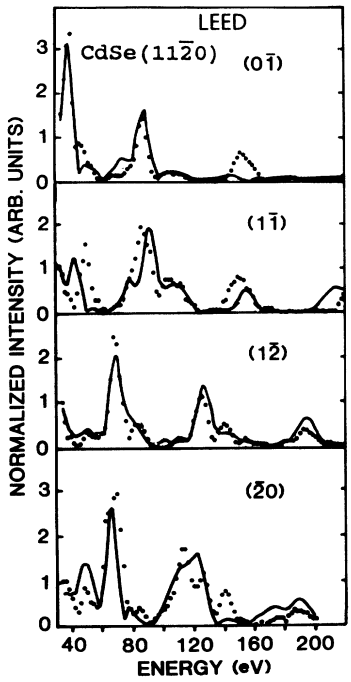

FIG. 18. Comparison of calculated and measured LEED intensities from CdSe(11$\bar{2}$0). The (0$\bar{1}$), (1$\bar{1}$), and ($\bar{2}$0) beams are representative of the strong beams [(0$\bar{1}$), (1$\bar{1}$), ($\bar{2}$0), and ($\bar{1}\bar{1}$)]; the (1–2) beam is representative of the moderate intensity beams [(20), ($\bar{1}\bar{2}$), (1–2), (0,–2), and ($\bar{2}\bar{1}$)]; the (0$\bar{3}$), (2$\bar{1}$), ($\bar{1}\bar{3}$), and (1$\bar{3}$) beams are weak. The sample was held at a temperature of 110 K.

(22)=(2$\bar{2}$) beams. While some small improvements in the convergence of the line shapes was observed upon including up to five layers treated exactly, three exact layers was deemed adequate to perform the structural search, while the final best-fit structure was recalculated using four exact layers.

Once optimized values of V_i and $d_{12,\perp}$ were incorporated into the analysis, the scan of R_X versus ω was repeated. With the exception of a slight local minimum in R_X at $\omega = 10°$ being shifted to $\omega = 5°$, the shape of the curves are nearly identical. Figure 15 shows the resulting scan over ω, as well as the analogous ones for LEED. Figure 16 gives the dependence of R_I on ω analogous to Fig. 15. The minimum for LEPD is quite sharp, similar to the results for CdSe(10$\bar{1}$0).

Variations in the remaining independent surface structure parameters failed to improve the fits significantly. The various best-fit structures are specified in Table II. A comparison of calculated and measured intensities is given in Fig. 17 for LEPD. A comparison between the calculated intensities and the Princeton LEED data is shown in Fig. 18, utilizing Princeton's best-fit structure to these data. The visual correspondence between the two is much better than suggested by the numerical value of R_X.

VI. DISCUSSION

We have shown in the preceding sections that complete R-factor structure analyses for CdSe(10$\bar{1}$0) and CdSe(11$\bar{2}$0) can be successfully performed using both LEED and LEPD. The LEED analyses were performed independently using different intensity data and separate calculations performed by different people at different institutions. The essentially identical R-factor curves (Figs. 8, 9, 15, and 16) and best-fit structures (Tables I and II) that emerge from these analyses demonstrate both the reproducibility of the measurements and the robustness of the analysis procedure. Moreover, for CdSe(10$\bar{1}$0) our present analysis also reproduces the re-

TABLE II. Structural variables and associated R factors as determined by (a) LEPD and (b) LEED for the CdSe(11$\bar{2}$0) surface. Distances are measured in angstroms; ω is measured in degrees; R_X and R_I are dimensionless. The results for four structural models are shown: unreconstructed (bulk terminated), best bond-length conserving relaxation (via R_X minimization), best fit (via R_X minimization), and theory [Wang *et al.* (Ref. 64)]. Princeton data are labeled with an asterisk.

	$\Delta_{1,\perp}$	$\Delta_{1,x}$[a]	$\Delta_{1,y}$[b]	$d_{12,\perp}$	$d_{12,x}$[c]	$\Delta_{2,\perp}$[d]	ω	R_X	R_I
				(a) LEPD					
Unreconstructed	0	2.64	0	2.15	3.51	0	0	0.22	0.25
Best ω	0.61	2.51	0.52	1.71	3.74	0	27°	0.14	0.03
Best fit	0.61	2.51	0.52	1.62	3.74	–0.02	27°	0.12	0.04
Theory	0.73	2.43	0.51	1.55	3.84	–0.11	32°		
				(b) LEED					
Unreconstructed	0	2.64	0	2.15	3.51	0	0	0.39*	0.20*
Best fit Princeton	0.76	2.46	0.55	1.47	3.81	0	34°	0.29	0.12
Best fit Brandeis	0.73	2.47	0.55	1.51	3.80	0	33°	0.32	0.22
Theory	0.73	2.43	0.51	1.55	3.84	–0.11	32°		

[a]Labeled $a_y - \Delta_{1,y}$ in Ref. 64 because a different coordinate system was used.
[b]Labeled $\Delta_{1,x}$ in Ref. 64.
[c]Labeled $d_{12,y}$ in Ref. 64.
[d]Labeled $-\Delta_{2,\perp}$ in Ref. 64 because of a different sign convention.

sults of an earlier analysis by Duke *et al.*[11] to within the expected errors (±0.05 Å for top-layer displacements normal to the surface and ±0.2 Å for top-layer displacements parallel to the surface).

It is, however, evident that the LEPD analyses yield optimal fits at significantly (> 0.1 Å) smaller top-layer relaxations than do the LEED analyses. One could argue that the R_X minima in LEPD are sufficiently broad that the LEPD and LEED structures indeed agree within stated uncertainties; however, in principle such conclusions could depend upon the choice of R factor used to optimize the independent structural variables. For example, the form of the x-ray R factor R_X used in this work [defined by Eqs. (3), (8), (13), (14), and (16) of Ref. 62] ignores the relative intensities of individual beams by using separate normalization factors which normalize the integrated intensities of $I_{\rm th}(V)$ and $I_{\rm expt}(V)$ separately for each beam. Inspection of Figs. 9 and 16 would, however, suggest that some valuable structural information may be contained within the relative intensities of nondegenerate beams; these figures indicate that the integrated beam R factor R_I in LEPD exhibits a stronger dependence on the principal independent structural variable ω than it does on R_X. Therefore, we have recalculated the R_X-versus-ω plots for the (10$\bar{1}$0) and (11$\bar{2}$0) surfaces using a version of R_X which entails a *single, global* normalization factor C for all beams. The resulting "global" R factor R_X is calculated by the same prescription for R_X given by Eqs. (6)–(9), with the notable exception that instead of normalizing $I_{\rm th}^{(i)}(E)$ to $I_{\rm expt}^{(i)}(E)$ for each beam, all normalization constants C_i are the same. Thus for R_{XG}, Eq. (9) is replaced with

$$\frac{\partial R_{XG}}{\partial C} = 0 \ , \tag{21}$$

and $C_i = C$ for all beams. This choice of R factor seems validated by the assertion that, if the theory is expected to accurately predict the intensity line shapes of the individual beams, one would also expect it to reproduce the relative intensities of the individual beams as well.[63,66]

The variation of the R_{XG} with ω is indicated by Figs. 19 and 20 for the (10$\bar{1}$0) and (11$\bar{2}$0) surfaces, respectively. Comparison of these with Figs. 8 and 15 (corresponding to the results of the earlier form of R_X) leads to the following conclusions: (1) The LEPD minima are now somewhat sharper than the corresponding LEED minima, rather than being considerably broader. (2) The overall agreement between calculated and measured intensities, as indicated by the magnitude of the R factors, is significantly better for LEPD than for LEED for R_X as well as R_{XG}. (3) The conclusions of the structural search are only slightly modified, with the best-fit ω for LEPD shifting from $\omega = 15° \pm 5°$ to $\omega = 17° \pm 3°$ for the (10$\bar{1}$0) surface; the (10$\bar{1}$0) LEED ω values are likewise shifted slightly from their previously congruent value of $\omega = 21.5° \pm 3°$, with the Brandeis and Princeton minima moving apart to $\omega = 20° \pm 3°$ and $\omega = 22° \pm 3°$, respectively. For the (11$\bar{2}$0) surface, the Princeton LEED minimum suggests a best-fit value of $\omega = 32° \pm 4°$ versus its previous value of $\omega = 34° \pm 3°$, while the Brandeis

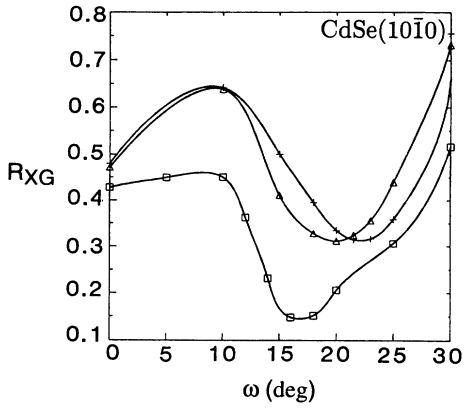

FIG. 19. Variations in the LEED and LEPD globally normalized x-ray R factor associated with bond-length-conserving rotations ω of the top-layer dimers for CdSe(10$\bar{1}$0), for comparison with Fig. 8. Squares: LEPD. Triangles: Brandeis LEED. Crosses: Princeton LEED.

LEED remains at its previous value of $\omega = 33° \pm 5°$. The LEPD minimum, however, is shifted from $\omega = 27° \pm 5°$ to $\omega = 26° \pm 3°$. (4) The LEED and LEPD structures still appear close to being compatible within the stated uncertainties. Thus, in this case the structural conclusions are not seriously affected by the choice of normalization for R_X.

Although the same scattering theory is successfully used to describe both LEED and LEPD, there are many interesting differences in the way electrons and positrons interact with the muffin-tin potential of the crystal, as briefly described by Horsky *et al.*[6] and more formally presented in a definitive study by Duke and Lessor.[32] For example, in the angular momentum representation the ion-core partial-wave potentials $V_l(r)$ are expressed as the sum of the ion-core potential $V_a(r)$ and the repulsive centrifugal barrier term $V_c(r,l) = \hbar^2 l(l+1)/2mr^2$, i.e., $V_l(r) = V_a(r) + V_c(r,l)$.[32,67] For electrons, the compe-

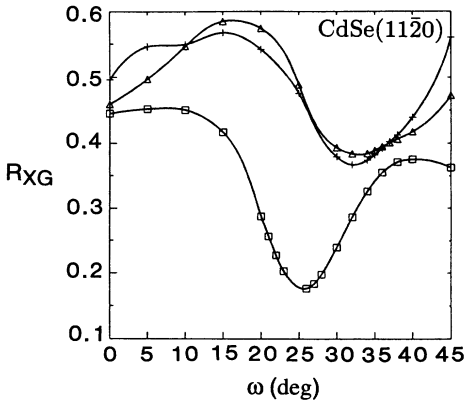

FIG. 20. Variations in the LEED and LEPD globally normalized x-ray R factor associated with bond-length-conserving relaxations of the top layer (denoted by ω) for CdSe(11$\bar{2}$0), for comparison with Fig. 15. Squares: LEPD. Triangles: Brandeis LEED. Crosses: Princeton LEED.

tition between the attractive $V_a(r)$ and repulsive $V_c(r,l)$ results in a significant amplitude of the electron wave function near the ion core for small values of the angular momentum l; the terms being of opposite sign also result in bound-state resonances for higher values of l. For positrons, however, both terms of $V_l(r)$ are positive, so that the positron wave function is maximal much farther from the ion core and hence is much less sensitive to the exact form of $V_a(r)$. Consequently, the poorly defined positron–core-electron correlation interaction is much reduced, eliminating it as a significant source of error in the determination of $V_a(r)$.

The positive definite form of $V_a(r)$ leads to positron phase shifts and scattering cross sections which are relatively insensitive to elemental specificity (i.e., they are nearly the same for Cd and Se), in sharp contrast to the very different phase shifts and scattering cross sections exhibited by electrons for elements in different rows and columns of the Periodic Table.[6,32,38]

This fact can help to explain the strong sensitivity of R_I to the primary structural variable ω in LEPD. Since positron scattering from the anion and cation is very similar, one can view the unrelaxed, bulk-terminated surface to a first approximation as consisting of effectively one species of scatterer for LEPD. In this case, the surface possesses a higher degree of symmetry, leading to reduced scattering into certain beams. As the surface relaxes, this artificial symmetry is broken, so that the relative beam strength in LEPD would be highly sensitive to the degree of relaxation: a prediction compatible with our observation of a factor of 4–15 reduction in $I_{\rm th}(V)$ for the (01), $(0\bar{1})$, (11), and $(1\bar{1})$ beams for the $(10\bar{1}0)$ surface as ω is reduced towards zero in the calculations.

A further point of difference between the crystal potential seen by the e^- and e^+ is in the value of the real part of the optical potential, V_0. For most materials, the positron V_0 is within a few eV of zero, making possible negative work-function materials for use as slow-positron moderators.[68] Since the electron V_0 is much larger, e.g., 12 eV (e^-) versus 2 eV (e^+) for CdSe, so also is its absolute uncertainty. Since many LEED workers believe that V_0 is a function of the magnitude[69] and possibly the direction of the incident electron wave vector, and since also the falloff of V_0 at the crystal surface is not typically included in LEED calculations for structure analysis, the small value of V_0 for positrons is undoubtably an advantage. For example, the systematically larger perpendicular displacements deduced by LEED versus LEPD in this work could be related to the physical variation of the electron de Broglie wavelength at the crystal surface, which would be a negligible effect for the positron. If $V_0(\text{surface}) \ll V_0(\text{bulk})$, the e^- would have a longer de Broglie wavelength in the vicinity of the surface, perhaps leading to larger deduced displacements of the surface atoms.

The absorptive or imaginary part of the optical potential V_i is associated with the inelastic mean free path, λ_{ee}. As previously discussed, best agreement with experiment was obtained using a constant value of λ_{ee} for electrons and an energy-dependent form (represented by a constant value of V_i) for positrons. The positron λ_{ee} is found to be smaller than that of the electron; this result is likely due to the same mechanism responsible for the differences in the electron and positron mean free paths in metals.[29] Briefly, we can view the inelastic scattering of LEED-energy electrons in metals as being determined by the density of occupied states (in the case of electron-hole pair creation), as well as by the availability of unoccupied states for the scattered electrons. However, there are no excluded final states for the positron, since there is only one positron at a time in the sample. In the free-electron approximation, this results in a 30% reduction in λ_{ee} as compared to that of electrons at 50 eV, for example.[29] Although one would expect the lack of excluded states to play a similar role in reducing the positron λ_{ee} in nonmetals, it is not a simple matter to extrapolate the results of the jellium model to such systems. Recently, Tanuma, Powell, and Penn calculated the electron λ_{ee} for non-free-electron-like materials.[70,71] In the future these calculations can hopefully be extended to include positrons in semiconductors. The question of the positron versus the electron λ_{ee} in semiconductors is not only of fundamental interest for understanding electronic collisions in solids, but is particularly important with regard to assessing the relative surface sensitivity of LEPD versus LEED in the structural determination of semiconductors and insulators. In particular, our CdSe results might be a reflection of the reduced sensitivity of LEPD to subsurface layers. If there is the possibility of complex subsurface relaxations that have yet to be included in the structure search and incorporated into the $I_{\rm th}(V)$ calculations, then the better agreement between theory and experiment for positrons could be a simple consequence of the shorter positron λ_{ee}.

VII. CONCLUSIONS

The important conclusion to emerge from our analysis is that CdSe$(11\bar{2}0)$ is relaxed in accordance with prior theoretical predictions.[17,64] The complicated structure of this surface preserves the glide-plane symmetry in both the model predictions and the experimental measurements. The resulting local coordination chemistry of both the anion and cation remains the same for zinc-blende (110) surfaces, for CdSe$(10\bar{1}0)$, and for CdSe$(11\bar{2}0)$. Moreover, the combination of the topological possibility of bond-length-conserving surface relaxations and the surface-state-lowering mechanism which generates the driving force for the surface-bond rehybridization is reaffirmed as the "cause" of this universal surface coordination on the relaxed cleavage surfaces of tetrahedrally coordinated compound semiconductors.

Although Figs. 8 and 15 reveal different structures associated with the absolute minima in R_X, our error analysis suggests that the LEED and LEPD structures are indeed compatible within the established uncertainties. Given the reproducibility of the LEED intensities and R_X-versus-ω curves, it is comforting to recognize that the difference between the R_X-versus-ω curves for LEED and LEPD reflect differences in the physical interactions of these entities with the solid surface, which

nevertheless yield compatible surface atomic geometries when known uncertainties are incorporated into the analysis. Moreover, the fact that LEED theory yields an improved agreement between theoretical and experimental *I-V* profiles, when applied to positrons, may offer further insight that could aid in providing more accurate *I-V* calculations for electrons in the future. Indeed, the goal of this methodology should be the combination of both e^- and e^+ measurements to yield a *single* structure possessing a higher confidence level than presently attainable by either spectroscopy alone.

ACKNOWLEDGMENTS

This work was supported in part by NSF Grants No. DMR-8519524 and No. DMR-8709531. The Pacific Northwest Laboratory is operated by the Battelle Memorial Institute for the Department of Energy under Contract No. DE-AC06-76RLO 1830.

*Present address: Balzer High Vacuum Products, 8 Sagemore Park Rd., Hudson, NH 03051.
†Present address: Advanced Technology Materials, Inc., 7 Commerce Drive, Danbury, CT 06810.

[1]C.B. Duke, J. Vac. Sci. Technol. A **6**, 1957 (1988).
[2]C.B. Duke, in *Surface Properties of Electronic Materials*, edited by D.A. King and D.P. Woodruff (Elsevier, Amsterdam, 1988), pp. 69–118.
[3]A. Kahn, Surf. Sci. Rep. **3**, 193 (1983).
[4]C.B. Duke and Y.R. Wang, J. Vac. Sci. Technol. A **6**, 692 (1988).
[5]C.B. Duke, D.L. Lessor, T.N. Horsky, G. Brandes, K.F. Canter, P.H. Lippel, A.P. Mills, Jr., A. Paton, and Y.R. Wang, J. Vac. Sci. Technol. A **7**, 2030 (1989).
[6]T.N. Horsky, G.R. Brandes, K.F. Canter, C.B. Duke, S.F. Horng, A. Kahn, D.L. Lessor, A.P. Mills, Jr., A. Paton, K. Stevens, and K. Stiles, Phys. Rev. Lett. **62**, 1876 (1989).
[7]K.F. Canter, C.B. Duke, and A.P. Mills, in *Chemistry and Physics of Solid Surfaces VIII*, edited by R. Vanselow and R. Howe, Springer Series in Surface Sciences Vol. 22 (Springer-Verlag, Berlin, 1990), p. 183.
[8]P. Mark, S.C. Chang, W.F. Creighton, and B.W. Lee, Crit. Rev. Solid State Sci. **5**, 189 (1975).
[9]C.B. Duke, A.R. Lubinsky, S.C. Chang, B.W. Lee, and P. Mark, Phys. Rev. B **15**, 4865 (1977).
[10]C.B. Duke, R.J. Meyer, A. Paton, and P. Mark, Phys. Rev. B **18**, 4255 (1978).
[11]C.B. Duke, A. Paton, Y.R. Wang, K. Stiles, and A. Kahn, Surf. Sci. **197**, 11 (1988).
[12]C.B. Duke and Y.R. Wang, J. Vac. Sci. Technol. B **6**, 1440 (1988).
[13]J.P. LaFemina and C.B. Duke, J. Vac. Sci. Technol. A **9**, 1847 (1991).
[14]Y.R. Wang and C.B. Duke, Surf. Sci. **192**, 309 (1987).
[15]Y.R. Wang, C.B. Duke, and C. Mailhiot, Surf. Sci. Lett. **188**, L708 (1987).
[16]Y.R. Wang and C.B. Duke, Phys. Rev. B **36**, 2763 (1987).
[17]Y.R. Wang and C.B. Duke, Phys. Rev. B **37**, 6417 (1988).
[18]I.J. Rosenberg, A.H. Weiss, and K.F. Canter, Phys. Rev. Lett. **44**, 1139 (1980).
[19]C. Davisson and L.H. Germer, Phys. Rev. **30**, 705 (1927).
[20]P.J. Schultz and K.G. Lynn, Rev. Mod. Phys. **60**, 701 (1988).
[21]A.P. Mills, Jr., Appl. Phys. **23**, 189 (1980).
[22]K.F. Canter, in *Positron Scattering in Gases*, edited by J.W. Humberston and M.R.C. McDowell (Plenum, London, 1984), pp. 219–225.
[23]K.F. Canter, G.R. Brandes, T.N. Horsky, P.H. Lippel, and A.P. Mills, Jr., in *Atomic Physics with Positrons*, edited by J.W. Humberston and E.A.G. Armour (Plenum, London, 1987), pp. 153–160.
[24]K.F. Canter and A.P. Mills, Jr., Can. J. Phys. **60**, 551 (1982).
[25]W.E. Frieze, D.W. Gidley, and K.G. Lynn, Phys. Rev. B **31**, 5628 (1985).
[26]R. Mayer, C.-S. Zhang, K.G. Lynn, W.E. Frieze, F. Jona, and P.M. Marcus, Phys. Rev. B **35**, 3102 (1987).
[27]A.H. Weiss, I.J. Rosenberg, K.F. Canter, C.B. Duke, and A. Paton, Phys. Rev. B **27**, 867 (1983).
[28]R. Mayer, C-Si Zhang, K.G. Lynn, J. Throwe, P.M. Marcus, D.W. Gidley, and F. Jona, Phys. Rev. B **36**, 5659 (1987).
[29]J. Oliva, Phys. Rev. B **21**, 4909 (1980).
[30]R. Feder, Solid State Commun. **34**, 541 (1980).
[31]F. Jona, D.W. Jepsen, P.M. Marcus, I.J. Rosenberg, A.H. Weiss, and K.F. Canter, Solid State Commun. **36**, 957 (1980).
[32]C.B. Duke and D.L. Lessor, Surf. Sci. **225**, 81 (1990).
[33]M.N. Read and D.N. Lowy, Surf. Sci. **107**, L313 (1981).
[34]M.N. Read and G.J. Russell, Surf. Sci. **88**, 95 (1979).
[35]A. Vehanen, K.G. Lynn, P.J. Schultz, and M. Eldrup, Appl. Phys. A **32**, 163 (1983).
[36]K.F. Canter, P.H. Lippel, W.S. Crane, and A.P. Mills, Jr., in *Positron Studies of Solids, Surfaces, and Atoms: A Symposium to Celebrate Stephan Berko's 60th Birthday*, edited by A.P. Mills, Jr., W.S. Crane, and K.F. Canter (World Scientific, Singapore, 1986), pp. 199–206.
[37]D.W.O. Heddle and N. Papadovassilakis, J. Phys. E **17**, 599 (1983).
[38]T.N. Horsky, Ph.D. thesis, Brandeis University, 1988 (University Microfilms, Ann Arbor, MI).
[39]6-in. 120° display LEED grids supplied by Perkin-Elmer, Physical Electronics Division, Eden Prairie, MN.
[40]Galileo Electro-Optics, Sturbridge, MA.
[41]Surface Science Laboratories, Palo Alto, CA.
[42]J.L. Wiza, Nucl. Instrum. Methods **162**, 587 (1979).
[43]Cleveland Crystals, Cleveland, OH.
[44]Type M Microcircuit Silver (Transene Co. Inc., Rowley, MA).
[45]R. Lee, Iguana Systems, Framingham, MA.
[46]H.L. Davis and J.R. Noonan, Phys. Scr. **T4**, 141 (1983).
[47]D.A. Liberman, J.T. Waber, and D.T. Cromer, Phys. Rev. **137**, A27 (1965).
[48]D.A. Liberman, D.T. Cromer, and J.T. Waber, Comput. Phys. Commun. **2**, 107 (1971).
[49]J.C. Slater, Phys. Rev. **81**, 385 (1951).
[50]W. Kohn and L.J. Sham, Phys. Rev. **140**, A1133 (1965).
[51]S. Hara, J. Phys. Soc. Jpn. **22**, 710 (1967).
[52]R.J. Meyer, C.B. Duke, and A. Paton, Surf. Sci. **97**, 512 (1980).
[53]W.K. Ford, C.B. Duke, and A. Paton, Surf. Sci. **115**, 195 (1982).
[54]C.B. Duke, A. Paton, Y.R. Wang, K. Stiles, and A. Kahn, Surf. Sci. **214**, 334(E) (1989).
[55]D.W. Jepsen, P.M. Marcus, and F. Jona, Phys. Rev. B **5**,

3933 (1972).
[56]C.F. Cline, H.L. Dunegan, and G.W. Henderson, J. Appl. Phys. **38**, 1944 (1967).
[57]A. Mitsuishi, H. Yoshinaga, and S. Fujita, J. Phys. Soc. Jpn. **13**, 1235 (1958).
[58]C.B. Duke, Adv. Chem. Phys. **27**, 1 (1974).
[59]R.J. Meyer, C.B. Duke, A. Paton, A. Kahn, E. So, J.L. Yeh, and P. Mark, Phys. Rev. B **19**, 5194 (1979).
[60]A. Kahn, C.B. Duke, and Y.R. Wang, Phys. Rev. B **44**, 5606 (1991).
[61]G.E. Laramore and C.B. Duke, Phys. Rev. B **5**, 267 (1972).
[62]E. Zanazzi and F. Jona, Surf. Sci. **62**, 61 (1977).
[63]C.B. Duke, S.L. Richardson, and A. Paton, Surf. Sci. **127**, L135 (1983).
[64]Y.R. Wang, C.B. Duke, K. Stevens, A. Kahn, K.O. Magnusson, and S.A. Flodström, Surf. Sci. **206**, L817 (1988).
[65]C.B. Duke, A. Paton, W. K. Ford, A. Kahn, and J. Carelli, Phys. Rev. B **24**, 562 (1981).
[66]D.M. Lind, F.B. Dunning, G.K. Walters, and H.L. Davis, Phys. Rev. B **35**, 9037 (1987).
[67]L.I. Schiff, *Quantum Mechanics*, 2nd ed. (McGraw-Hill, New York, 1955), pp. 103–114.
[68]A.P. Mills, Jr., in *Positron Solid-State Physics*, edited by W. Brandt and A. Dupasquier (North-Holland, Amsterdam, 1983), pp. 423–509.
[69]P.J. Jennings and S.M. Thurgate, Surf. Sci. **104**, L210 (1981).
[70]S. Tanuma, C.J. Powell, and D.R. Penn, Surf. Interface Anal. **11**, 577 (1988).
[71]S. Tanuma, C.J. Powell, and D.R. Penn, J. Vac. Sci. Technol. A **8**, 2213 (1990).